www.lajss.org
Latin American Journal of Solids and Structures 2 (2005) 321–337

A numerical inquiry into the flutter phenomenon in long-span bridges

E.S. Kreis* and J.C. André

Laboratory of Computational Mechanics, Department of Structural and Foundations Engineering Foundations, Escola Politécnica da Universidade de São Paulo, Av. Prof. Almeida Prado, Trav. 2, 85, 05508-900, São Paulo – SP, Brazil

Abstract

Due to their architectural characteristics and structural performance, cable-stayed and suspension bridges have become an increasingly usual choice where long-span bridges are required. This worldwide trend, dating from past decades, has also influenced Brazilian Engineering practices in the last few years. Several such structures are now either being designed or built in Brazil. One of the relevant aspects in the structural analysis of long-span bridges is their behavior under the influence of wind loads. Previous papers published by the authors dealt with the determination of critical wind speed corresponding to flutter instability, through the use of reduced mathematical models with two degrees of freedom. The structure was analyzed through the finite elements method and reduction was performed via superposition of modes selected to perform the best description of deck movement. Critical wind speed was then calculated through the determination of complex eigenvalues for several wind speeds. The present study is meant to go further. Flutter phenomena in long-span bridges are researched using time domain analysis and time series spectral analysis in order to determine vibration characteristics in the frequency domain. Those procedures are used to analyze the Normandy Bridge.

Keywords: Flutter, aeroelastic stability, cable-stayed bridge, suspension bridge, reduced mathematical model, mode superposition.

1 Foreword

Cable-stayed bridges are ever more present in several constructions in Brazil. They are both very elegant and slender, and are able to unite very distant margins, uniting them with spans which reach hundreds of meters.

Among the numberless cable-stayed bridges all over the world, one can refer to the Normandy bridge in France, (http://bridgepros.com/projects/LePontde%20Normandie/LePontdeNormandie.htm), which was completed and opened to public usage in 1995. This bridge has three spans, adding to a full length of 2,140 meters. The center span is 856 meter long, with a metallic section 624 meter long. This bridge presents a slenderness relation around 250 (span lenght on height of the

*Corresp. author Email: eri.kreis@poli.usp.br Received 26 September 2005; In revised form 11 October 2005

transversal section). At the time it was built, the Normandy bridge had the longest span in the world among cable-stayed bridges. This record was held until May, 1999 when the cable-stayed Tatara bridge, in Japan, was opened between Honshu and Shikoku, with three spans and a total length of 1,480 meters, and an 890 meter center span (http://www.hsba.go.jp/bridge/e-tatara.htm). Tatara bridge was a very successful project: in it, new technologies were used in research, design, fabrication and construction. This accomplishment must also contribute to make the dream of a 1,000 meter long span come true. For such slender bridges, studies of their behavior under wind action become relevant to the structural design, as shown by the collapse of the Tacoma Narrows bridge in 1940.

Previous studies [4, 6] developed in LMC – the Computational Mechanics Laboratory of Polytechnic School, São Paulo University, aimed at determining the critical wind speed corresponding to flutter instability. Structure discretizing was obtained through the finite element method and the drastic reduction of the number of degrees of freedom was achieved through the method of modal superposition. It should be pointed out that modal selection plays a central role in the good definition of a reduced mathematical model [5]. Flutter speed was obtained through the analysis of a problem of complex eigenvalues for several values of wind speed.

This paper amplifies those previous studies. Based on [1, 2], the flutter phenomenon is also studied by temporal analyses and by spectral analyses on time series. As Chen and Cai point out, these are not new procedures for analysis, but procedures which, when applied together, allow the follow up of the structure's response under wind action and, consequently, enable a better understanding of the occurrence of the flutter phenomenon. Considering the reduced mathematical model with two degrees of freedom, these procedures are applied to the study of the Normandy cable-stayed bridge.

2 Equations of motion for flutter analysis

2.1 Aerodynamic forces

Aerodynamic forces are defined in this paper according to the non-dimensional flutter derivatives, A_i^* e H_i^* $(i = 1, 4)$, for each bridge cross-section, through specific tests in wind tunnels [7].

In order to analyze vibrations in the longitudinal and vertical planes of the bridge under wind action with an uniform speed U, aerodynamic forces, lift forces L_v and pitch moment around x M_α, defined in a section of coordinate x, at instant t, are shown by:

$$\begin{aligned} L_v(x,t) &= \tfrac{1}{2}\rho U^2 B[KH_1^*\tfrac{\dot{v}(x,t)}{U} + KH_2^*\tfrac{B\dot{\alpha}(x,t)}{U} + K^2H_3^*\alpha(y,t) + K^2H_4^*\tfrac{v(x,t)}{B}] \\ M_\alpha(x,t) &= \tfrac{1}{2}\rho U^2 B^2[KA_1^*\tfrac{\dot{v}(x,t)}{U} + KA_2^*\tfrac{B\dot{\alpha}(x,t)}{U} + K^2A_3^*\alpha(x,t) + K^2A_4^*\tfrac{v(x,t)}{B}] \end{aligned} \tag{1}$$

where:

$K = \frac{B\omega}{U} = \frac{B(2\pi f)}{U}$ is the reduced frequency;

B is the deck width;

ω is the circular frequency of oscillation;

f is the frequency of oscillation;

$v\,(x,t)$ and $\alpha\,(x,t)$are the components of the dynamic parcel of vertical displacement and the angular displacement according to the longitudinal axis of a nodal point of the deck with an $x$coordinate, at instant t.

It is convenient to put (1) into a matricial shape

$$\left\{ \begin{array}{c} L_v \\ M_\alpha \end{array} \right\} = \frac{1}{2}\rho U^2 B \left[\begin{array}{cc} \frac{KH_1^*}{U} & \frac{KH_2^* B}{U} \\ \frac{KA_1^* B}{U} & \frac{KA_2^* B^2}{U} \end{array} \right] \left\{ \begin{array}{c} \dot{v} \\ \dot{\alpha} \end{array} \right\} + \frac{1}{2}\rho U^2 B \left[\begin{array}{cc} \frac{K^2 H_4^*}{B} & K^2 H_3^* \\ K^2 A_4^* & K^2 A_3^* B \end{array} \right] \left\{ \begin{array}{c} v \\ \alpha \end{array} \right\} \tag{2}$$

2.2 Equations of motion for the system discretized by the finite element method

The equations of motion for the system, which is characterized by a long-span bridge under a uniform wind action, discretized by the finite element method around the deformed equilibrium configuration, may be shown as:

$$\mathbf{M_0}\Delta\ddot{\mathbf{p}} + \mathbf{C_0}\Delta\dot{\mathbf{p}} + \mathbf{K_0}\Delta\mathbf{p} = \mathbf{P_A}\,(\Delta\dot{\mathbf{p}}, \Delta\mathbf{p}) \tag{3}$$

or, taking (2) into consideration,

$$\mathbf{M_0}\Delta\ddot{\mathbf{p}} + \mathbf{C_0}\Delta\dot{\mathbf{p}} + \mathbf{K_0}\Delta\mathbf{p} = \mathbf{C}_A\Delta\dot{\mathbf{p}} + \mathbf{K}_A\Delta\mathbf{p} \tag{4}$$

where, for the discrete system:

$\mathbf{M_0}$ is the mass matrix;

$\mathbf{C_0}$ is the damping matrix;

$\mathbf{K_0}$ is the stiffness matrix;

$\mathbf{C}_A$ is the matrix of aerodynamic damping;

$\mathbf{K}_A$ is the matrix of aerodynamic stiffness;

$\mathbf{\Delta p_A}$ is the displacement vector;

$\mathbf{P_A}$ is the vector of aerodynamic forces.

One should consider that in the type of bridge under study the deck's displacement is characterized by modes which basically mean bending and twisting. Since there is a great number of deck elements with the same ℓ length, displacements of the deck will be well defined by v_i, the vertical displacement of node i, and α_i, the rotation around the longitudinal direction of node i. Under these conditions, matrices $\mathbf{C_A}$ e $\mathbf{K_A}$ may described by:

$$\mathbf{C_A} = \left[\begin{array}{cccc} \mathbf{ca} & \mathbf{0} & \ldots & \mathbf{0} \\ \mathbf{0} & \mathbf{ca} & \ldots & \mathbf{0} \\ \vdots & \vdots & \ddots & \vdots \\ \mathbf{0} & \mathbf{0} & \ldots & \mathbf{ca} \end{array} \right] \qquad \mathbf{K_A} = \left[\begin{array}{cccc} \mathbf{ka} & \mathbf{0} & \ldots & \mathbf{0} \\ \mathbf{0} & \mathbf{ka} & \ldots & \mathbf{0} \\ \vdots & \vdots & \ddots & \vdots \\ \mathbf{0} & \mathbf{0} & \ldots & \mathbf{ka} \end{array} \right] \tag{5}$$

where:

$$\mathbf{ca} = \frac{1}{2}\rho U^2 B\ell \left[\begin{array}{cc} \frac{KH_1^*}{U} & \frac{KH_2^* B}{U} \\ \frac{KA_1^* B}{U} & \frac{KA_2^* B^2}{U} \end{array} \right] \qquad \mathbf{ka} = \frac{1}{2}\rho U^2 B\ell \left[\begin{array}{cc} \frac{K^2 H_4^*}{B} & K^2 H_3^* \\ K^2 A_4^* & K^2 A_3^* B \end{array} \right] \tag{6}$$

2.3 Equations of motion corresponding to the reduced mathematical model

The system reduction is established through the modal superposition method, which allows the establishment of:

$$\mathbf{\Delta p} = \mathbf{\Phi Y} \tag{7}$$

where $\mathbf{\Phi}$ is the modal matrix and $\mathbf{Y}$ is the vector of generalized modal coordinates.

By replacing (7) in (4) and multiplying to the left all the terms by $\mathbf{\Phi^T}$, one gets:

$$\mathbf{\Phi^T M_0 \Phi \ddot{Y}} + \mathbf{\Phi^T C_0 \Phi \dot{Y}} + \mathbf{\Phi^T K_0 \Phi Y} = \mathbf{\Phi^T} \mathbf{C}_A \mathbf{\Phi \dot{Y}} + \mathbf{\Phi^T} \mathbf{K}_A \mathbf{\Phi Y} \tag{8}$$

which may be turned into:

$$\mathbf{M_0^* \ddot{Y}} + \mathbf{C_0^* \dot{Y}} + \mathbf{K_0^* Y} = \mathbf{C_A^* \dot{Y}} + \mathbf{K_A^* Y} \tag{9}$$

In this study, two modes are selected according to the criteria established in [5], which allows one to establish:

$$\mathbf{\Delta p} = \mathbf{\Phi Y} = \boldsymbol{\phi_1} Y_1 + \boldsymbol{\phi_2} Y_2 \tag{10}$$

where ϕ_i is the modal vector corresponding to mode i and Y_i is its respective generalized modal coordinate. Equation (9) takes the following expanded form:

$$\begin{aligned} &\begin{bmatrix} 1 & 0 \\ 0 & 1 \end{bmatrix} \begin{Bmatrix} \ddot{Y}_1 \\ \ddot{Y}_2 \end{Bmatrix} + \begin{bmatrix} 2\xi_1\omega_1 & 0 \\ 0 & 2\xi_2\omega_2 \end{bmatrix} \begin{Bmatrix} \dot{Y}_1 \\ \dot{Y}_2 \end{Bmatrix} + \begin{bmatrix} \omega_1^2 & 0 \\ 0 & \omega_2^2 \end{bmatrix} \begin{Bmatrix} Y_1 \\ Y_2 \end{Bmatrix} = \\ &= \tfrac{1}{2}\rho U B \ell \mathbf{c a^*} \begin{Bmatrix} \dot{Y}_1 \\ \dot{Y}_2 \end{Bmatrix} + \tfrac{1}{2}\rho U^2 B \ell \mathbf{k a^*} \begin{Bmatrix} Y_1 \\ Y_2 \end{Bmatrix} \end{aligned} \tag{11}$$

where, by leaving aside terms with A_4^* e H_4^*:

$$\begin{aligned} ca_{ij}^* &= K \sum_{r=1}^{m} (H_1^* \phi_{2r-1,i} \phi_{2r-1,j} + B H_2^* \phi_{2r-1,i} \phi_{2r,j} + B A_1^* \phi_{2r,i} \phi_{2r-1,j} + B^2 K A_2^* \phi_{2r,i} \phi_{2r,j}) \\ ka_{ij}^* &= K^2 \sum_{r=1}^{m} (H_3^* \phi_{2r-1,i} \phi_{2r,j} + B A_3^* \phi_{2r,i} \phi_{2r,j}) \end{aligned} \tag{12}$$

with m representing the number of deck nodes.

3 Flutter analysis

3.1 Determining the flutter speed through complex eigenvalues

In order to determine the critical flutter speed, one should rewrite equation (9) in this form:

$$\mathbf{M_0^* \ddot{Y}} + (\mathbf{C_0^*} - \mathbf{C_A^*})\, \mathbf{\dot{Y}} + (\mathbf{K_0^*} - \mathbf{K_A^*})\, \mathbf{Y} = \mathbf{0} \tag{13}$$

The system's answer is taken as:

$$\mathbf{Y} = \mathbf{Y_0} e^{i\theta t} \text{ with } \theta = \Omega(U)(1 + i\varepsilon(U)) \tag{14}$$

where:

$\Omega(U)$ is the circular frequency of the system and

$\varepsilon(U)$ is the equivalent damping ratio of the system.

By introducing (14) into (13) and, after some algebraic transformations, the expressions corresponding to the following complex eigenvalue problems are obtained:

$$\left((\mathbf{K_0^*})^{-1}\mathbf{M}^* - \lambda\mathbf{I}\right)\mathbf{Y_0} = \mathbf{0} \tag{15}$$

where:

$$\mathbf{M}^* = I + i\frac{1}{\Omega(1+i\varepsilon)}\mathbf{C_A^*} + \frac{1}{\Omega^2(1+i\varepsilon)^2}\mathbf{K_A^*} \qquad \lambda = \frac{1 + \mathrm{i}2\xi(1+i\varepsilon)}{\Omega^2(1+i\varepsilon)^2} \tag{16}$$

The solution of (15) leads to two complex eigenvalues λ_1 e λ_2, which allows one to obtain effective modal frequencies Ω_j and the effective damping ratios ε_j of the aerodynamic system according to wind speed, through expressions:

$$\Omega_j(U) = \frac{1}{\sqrt{Re(\lambda_j)}} \qquad \varepsilon_j(U) = \xi - \frac{1}{2}\frac{Im(\lambda_j)}{Re(\lambda_j)} \tag{17}$$

By increasing wind speed U, flutter speed occurs for the value of U in which $\varepsilon(U)$ is no longer positive.

The solving of flutter coefficientes A_i^* and H_i^* for a given wind speed U cannot be done directly, since coefficients are dependent of the reduced frequencies K_1 (U,Ω (U)) and K_2 (U,Ω (U)). They are obtained by an iterative method with initial values$\bar{\Omega}_j = \omega_j$ and $\bar{K}_j = \frac{B\bar{\Omega}_j}{U}$, according to the procedure presented in the diagram of state presented in figure 5.

3.2 Determining flutter speed through temporal series

Temporal series $Y_1(t)$ and $Y_2(t)$ for several wind speeds are obtained by solving (11), which is done through the Runge-Kutta Method of order 4. The simple exam of $Y_i(t)$ for rising wind speeds allows the determination of flutter speed, characterized by divergence of this series.

Special attention should be paid to determining the modal frequencies and the modal damping ratios for a given speed, detailed in the state diagram of subsystem DREAMA in figure 5, for modal matrices $\mathbf{K_A^*}(U,K)$ e $\mathbf{C_A^*}(U,K)$ obtained from these values.

3.3 Spectral density or potency spectrum

With the temporal series of responses to vibration ranges $Y_1(t)$ e $Y_2(t)$ for rising wind speeds, the fast Fourier transform is applied in order to obtain the spectral density in the frequency domain, which assist in the interpretation of occurrence of the flutter phenomenon. The method used is the variant of the Cooley-Tukey algorithm.

4 The system developed for numerical inquiry

Numerical inquiry of the bridge deck behavior in order to analyse the flutter phenomenon in a long span bridge follows the conceptual procedure described in figure 1. Figures 2, 3 and 4 present respectively the functional diagrams of dependence among subsystems, of cases of usage of analysis process, and of collaboration of usage cases.

The discrete mathematical model is established through the finite element method. Modal analysis is accomplished using the ADINA® system.

Modal vectors and other information gathered from the discrete mathematical model are used to determine the modal selection parameters, according to criteria presented in [5]. Based on this information, established in subsystem PARMAS the modal selection is performed. Modelling of the aerodynamic stresses is done according to the description in item 2.1 and the definition of reduced aerodynamic actions is made according to expressions (4) and (5). It is then possible to build the reduced aeroelastyc mathematical model.

Flutter analysis by complex eigenvalues is achieved with the help of subsystem DREAMA which allows determination of effective frequencies and modal damping ratios and also of stiffness and aeroelastic damping for several wind speeds. The one corresponding to effective zero modal damping is the critical flutter speed. Details of this procedure are presented in figure 5 by the state diagram of subsystem DREAMA, which shows the sequence of steps for determination of damping ratios and modal frequencies.

The analysis of flutter by temporal series is achieved with the help of subsystem DoFETE, which uses the Runge-Kutta method of order 4 to numerically solve the reduced equations of motion.

Flutter analysis by espectral analysis in the frequency domain is done by applying the Fast Fourier Transform and considering the temporal series of generalized modal coordinates, processed by the same DoFETE subsystem.

Figure 6 shows the diagram for relationships among subsystems, as well as the interation between their data.

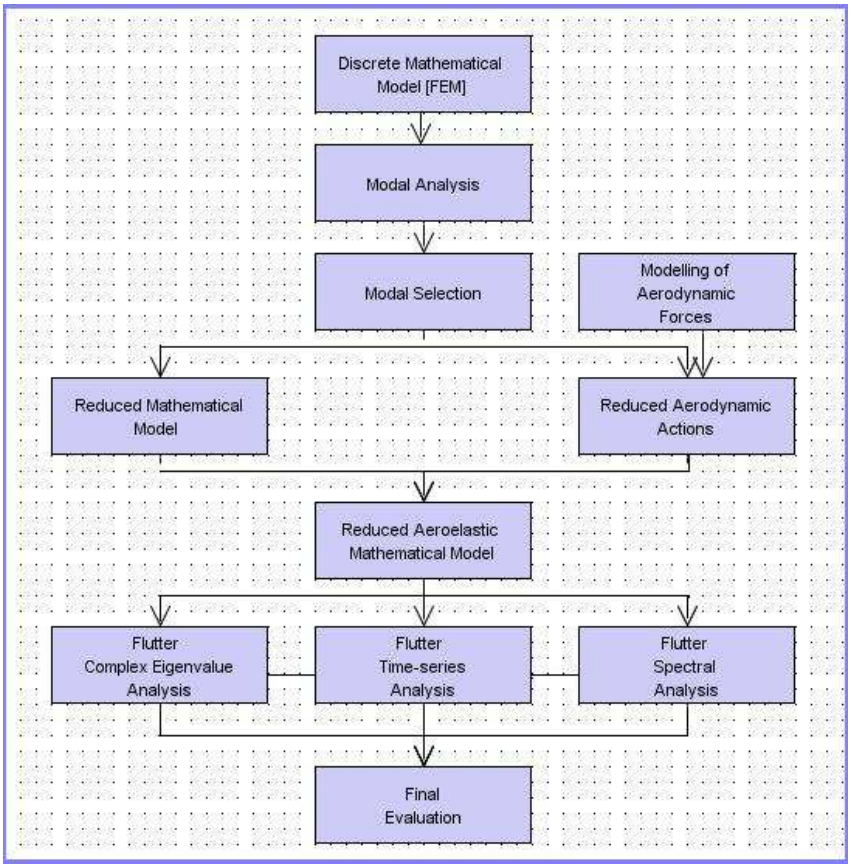

Figure 1: Conceptual Procedure

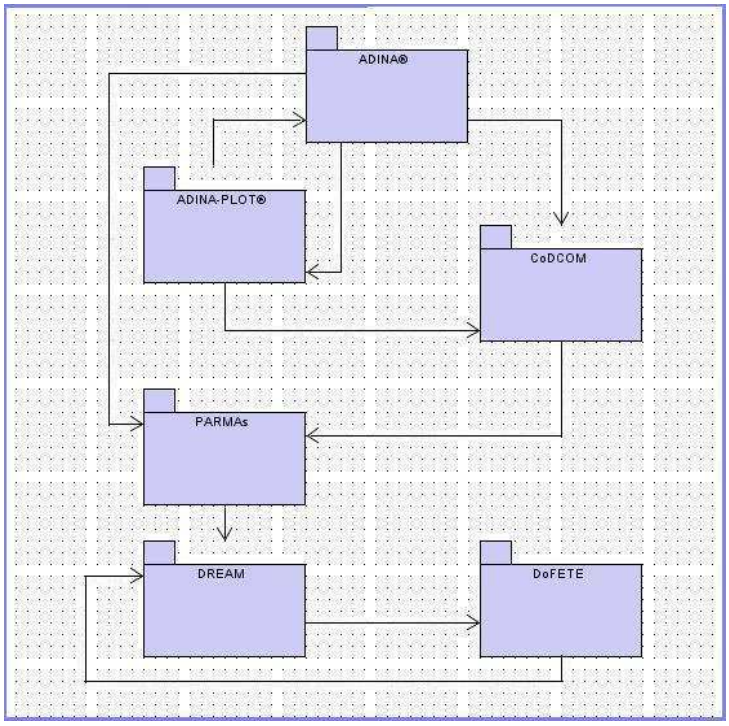

Figure 2: Diagram of functional procedure
Dependence among subsystems

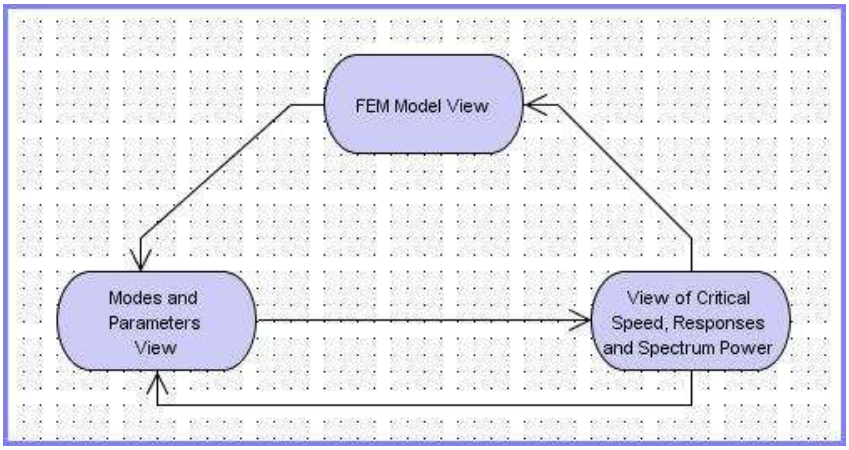

Figure 3: Diagram of functional procedure
Cases of usage of analysis process

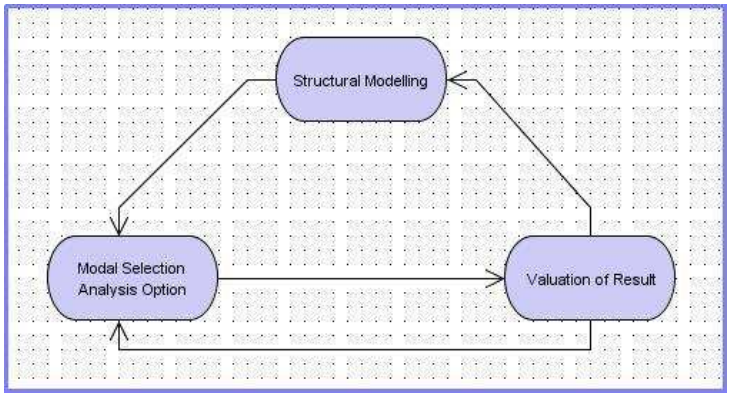

Figure 4: Diagram of functional procedure
Collaboration of usage cases

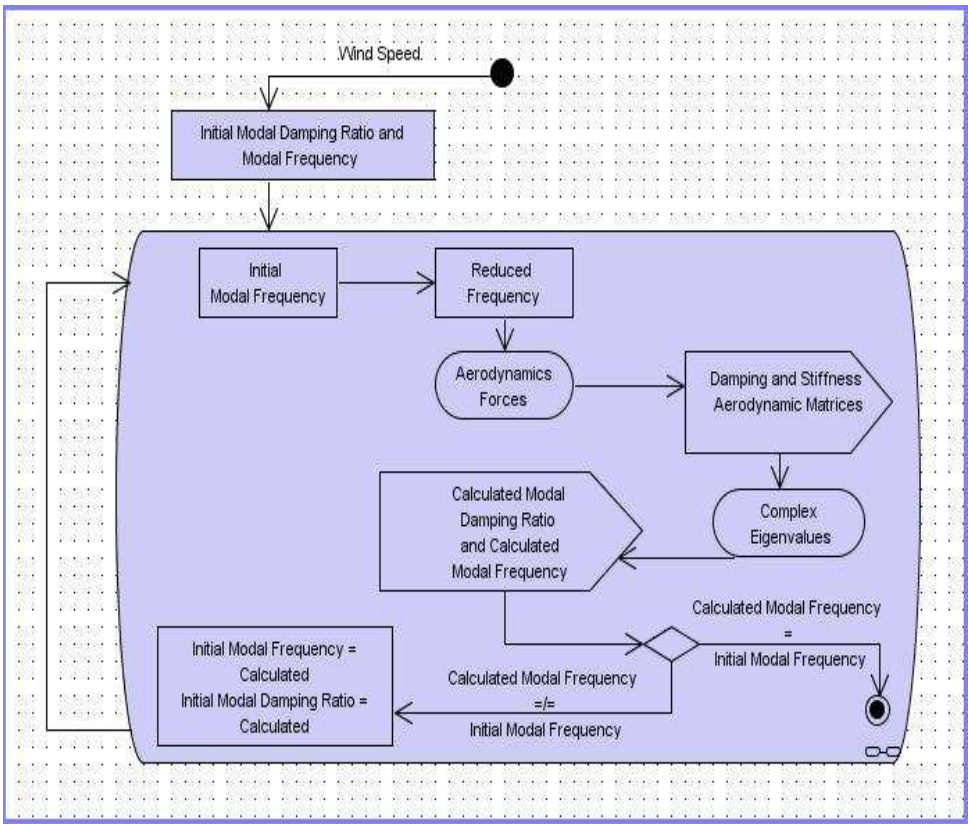

Figure 5: State Diagram of the DREAMA Subsystem

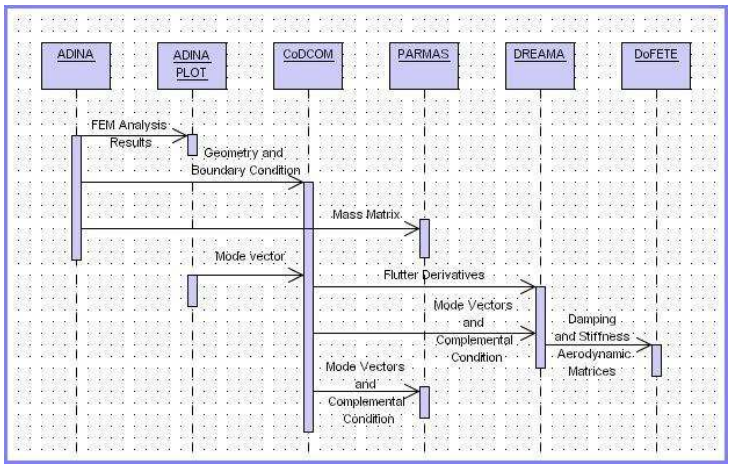

Figure 6: Diagram for interation sequence of system data

5 Case study: Cable-stayed bridge of Normandy

Data on the Normandy bridge are presented in [3,8]. Figures 7 and 8 show the lateral view and the transversal sections of the bridge deck.

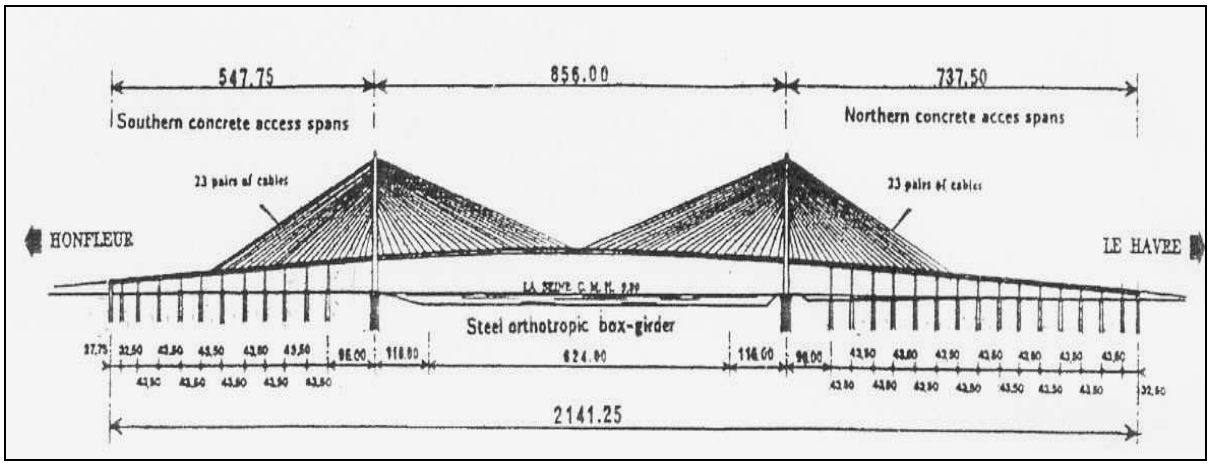

Figure 7: Lateral view of the Normandy bridge, [8].

In this paper, the Normandy bridge was discretized by spacial frame elements, there being 265 elements for the concrete segment of the deck, 125 elements for its steel segment and 80 elements for the two towers. Eighty spacial truss elements were used to simulate the cables.

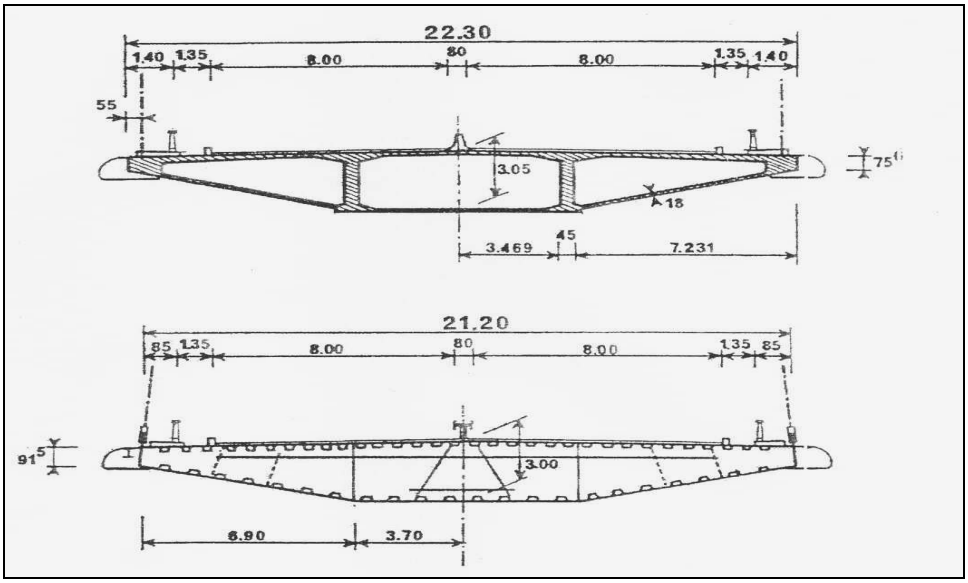

Figure 8: Transversal concrete sections (above) and steel sections (below) [8]

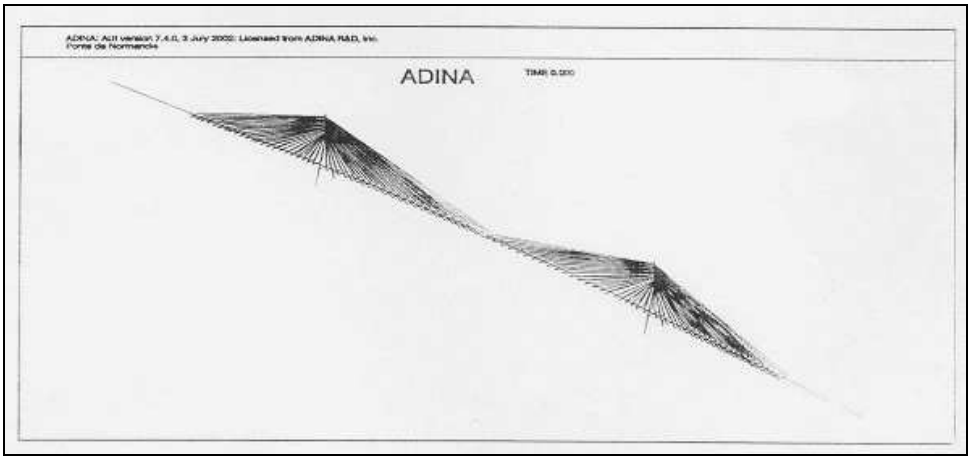

Figure 9: Discrete Mathematical Model of the Normandy Bridge

Additionally, 184 bar elements were used to help visualize vibration modes. Figure 9 shows a perspective of the discretized model. In the analyses run, the damping ratio was taken as 0.25%.

Modes 2 ($f_2 = 0.2376$ Hz) and 14 ($f_{14} = 0.8534$ Hz) were selected. These were held to be the most relevant ones for the flutter studies. Table 1 presents all modal parameters for the first 20 modes whose analysis led to the selection. It can be noticed that the first two modes which present a strong participation of the deck in the structure's movement ($R_2 = 0.9117$ and

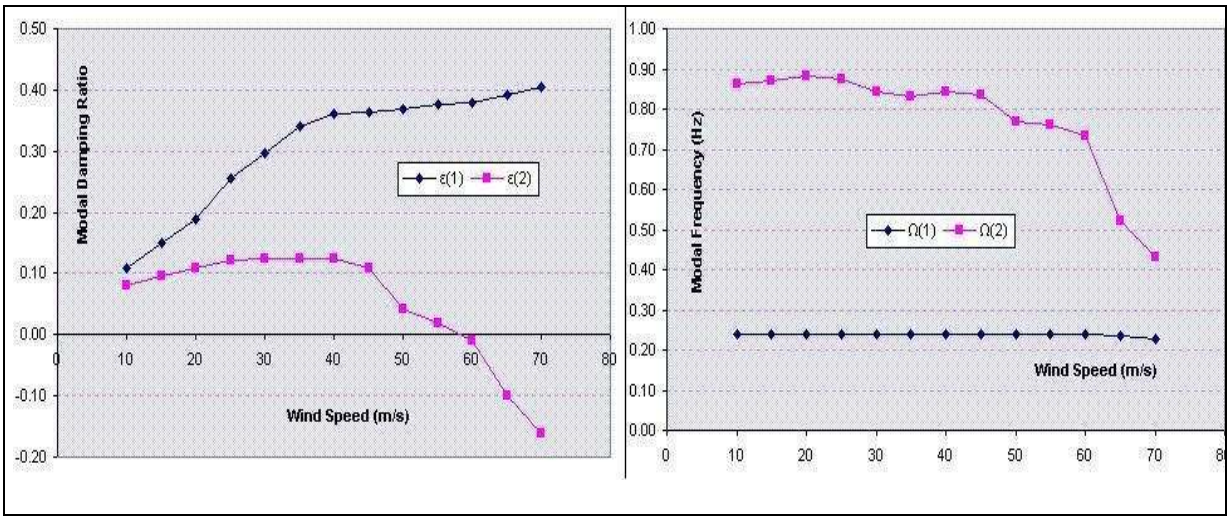

(a) (b)

Figure 10: Variance in the modal damping ratio and in effective modal frequencies regarding a uniform wind speed

Table 1: Modal parameters of the 20 modes for selection of two coupling modes

Mode	R	R_w	R_u	R_v	R_γ	R_α	R_β
1	0.9423	1.0000	0.0000	0.0000	0.0000	0.0000	0.0001
2	0.9117	0.0000	0.0002	0.9997	0.0001	0.0000	0.0000
3	0.9259	0.0000	0.0001	0.9995	0.0002	0.0000	0.0000
4	0.9622	0.9999	0.0000	0.0000	0.0000	0.0004	0.0005
5	0.9314	0.0000	0.0009	0.9984	0.0004	0.0000	0.0000
6	0.0079	0.4287	0.0000	0.0017	0.0000	0.5687	0.0004
7	0.0026	0.5315	0.0000	0.0001	0.0000	0.4662	0.0006
8	0.9316	0.0000	0.0032	0.9958	0.0006	0.0000	0.0000
9	0.9064	0.0002	0.0097	0.9889	0.0008	0.0000	0.0000
10	0.9379	0.9617	0.0000	0.0002	0.0000	0.0388	0.0009
11	0.8437	0.0000	0.0767	0.9214	0.0010	0.0000	0.0000
13	0.7416	0.0001	0.1137	0.8821	0.0014	0.0015	0.0000
14	0.7751	0.0761	0.0002	0.0014	0.0000	0.9220	0.0001
15	0.9038	0.0000	0.1994	0.7984	0.0014	0.0000	0.0000
16	0.6922	0.0000	0.1994	0.7984	0.0014	0.0000	0.0000
17	0.7203	0.0000	0.2320	0.7662	0.0010	0.0000	0.0000
18	0.8609	0.0000	0.1212	0.8759	0.0013	0.0000	0.0000
19	0.9512	0.0000	0.0377	0.9583	0.0020	0.0000	0.0000
20	0.6352	0.9858	0.0000	0.0000	0.0000	0.0144	0.0015

$R_{14} = 0.7751$) and, in the deck's movement, predominant vertical bending ($R_{v,2} = 0.9997$) and twisting ($R_{\alpha,14} = 0.9220$) are respectively modes 2 and 14.

Processing of the DREAMA subsystem was done for a rising sequence of speeds. Results are shown in Figure 10.

The wind speed which results in the modal damping ratio of zero twisting is 59m/s, which corresponds to the critical flutter speed. Figure 10b shows that the effective modal frequency associated to the vertical mode varies very little with speed oscillation. Also, the effective frequency associated to the twisting mode decreases with rising speed. It should be noticed there is no coalescence of the frequencies at the critical flutter speed.

Temporal analyses were made using the DoFETE subsystem, with initial conditions $Y_1(0) = 0.01$ m and $\dot{Y}_1(0) = 0.00$ m/s for mode 1 and $Y_2(0) = 0.01$ rd and $\dot{Y}_2(0) = 0.00$ rd/s for mode 2. Figure 11a shows the temporal series of vibration ranges $Y_1(t)$, associated to the first effective mode, with the rise of wind speed. Figure 11b shows the respective spectral densities of ranges. Figure 12a shows the temporal series of vibration ranges $Y_2(t)$, associated to the second effective mode, with the rising wind speed. Figure 12b shows the respective spectral densities of ranges. It can be noticed that the ranges of temporal series of $Y_1(t)$ e $Y_2(t)$ decrease rapidly for rising wind speeds up to approximately 45 m/s. Also, the system damping grows quite smaller for $U = 50$ m/s and, finally, these ranges grow in time up to $U = 60$ m/s, which characterizes an unstable state. Therefore it can be noticed that the critical flutter speed is inside the range 50 m/s $\leq U \leq 60$ m/s. It may be clearly observed in figures 11b and 12b, the dominion of the second mode in the system's response. There is no effective coalescence: what happens, in this case, is the dominion of the second effective mode, with $f_{2,effective} = 0.55$ Hz in the response in figure 13a.

Figure 13 shows the graphics of vibration ranges for the first and second effective modes and their respective spectral densities of ranges for $U = 40$ m/s and for the critical flutter speed $U_{fl} = 59$ m/s. It is important to observe in the flutter wind speed the absence of damping in the aerodynamic system and the dominion of the second effective mode in the system's response.

Acknowledgements: This paper is part of the result of a research project funded by CNPq. The authors thank CNPq for their financial support.

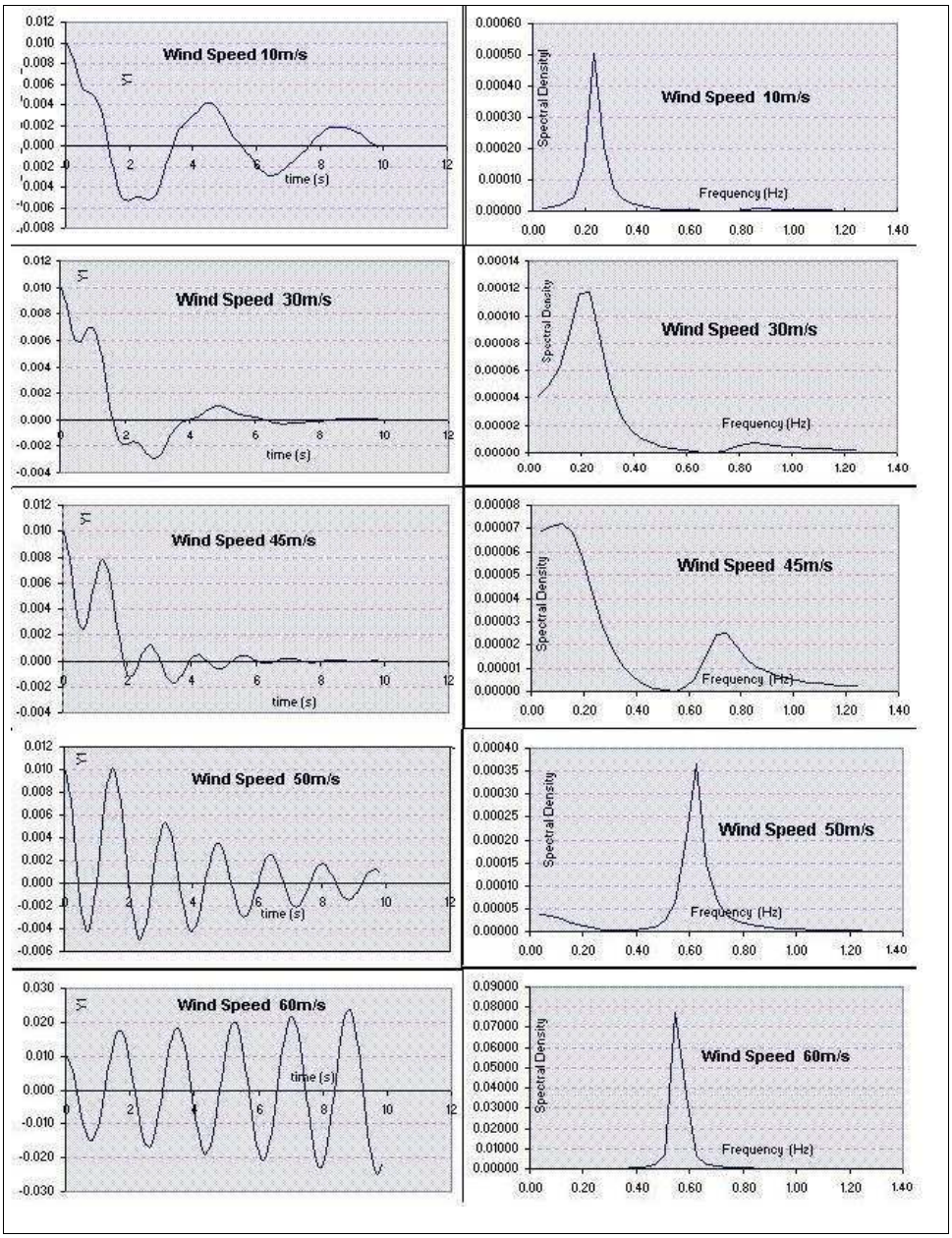

(a) (b)

Figure 11: Vibration ranges for the first effective mode and its respective spectral densities of ranges for several values of wind speed

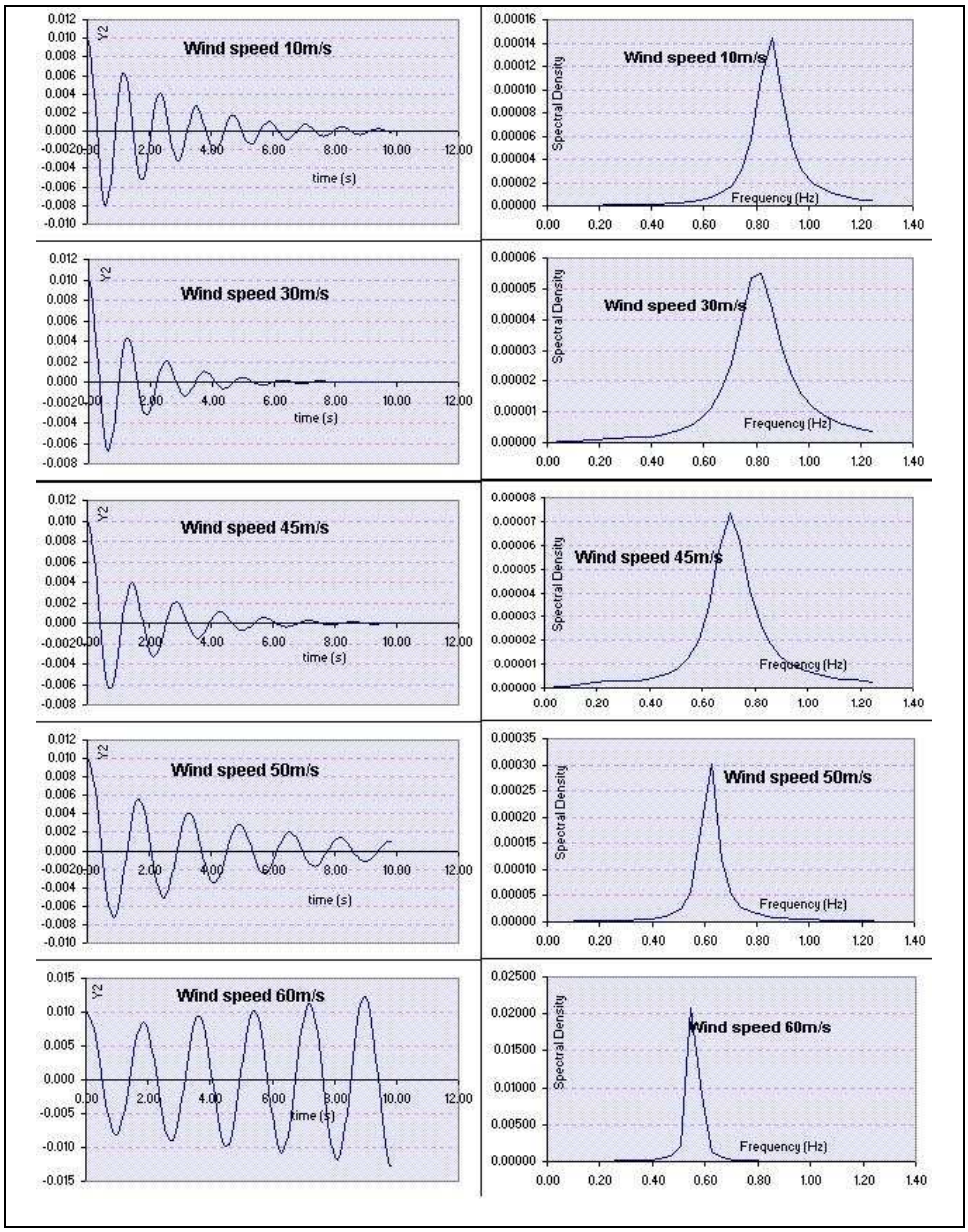

(a) (b)

Figure 12: Vibration ranges for the second effective mode and its respective spectral densities of ranges for several values of wind speed

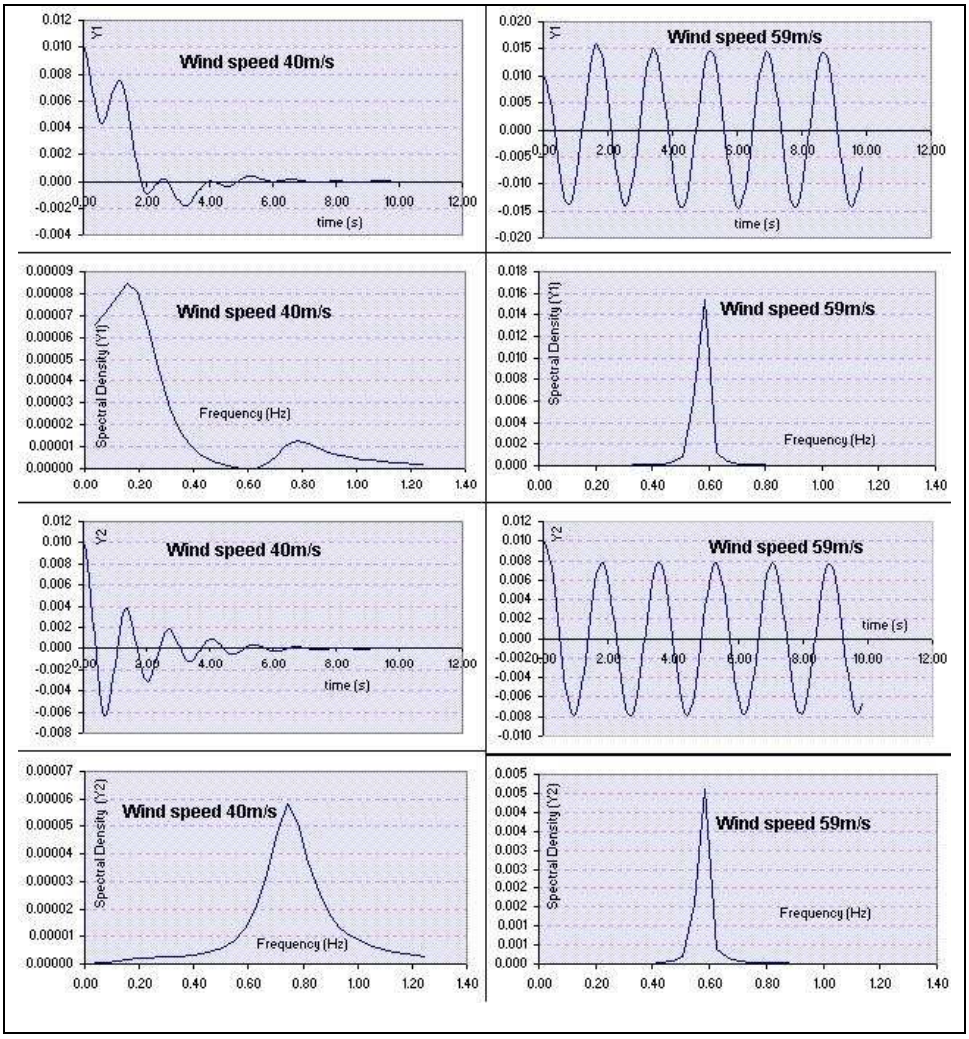

(a) (b)

Figure 13: Vibration ranges for the first and second effective modes and their respective spectral densities for $U = 40$ m/s and at the critical flutter speed $U_{dr} = 59$ m/s

References

[1] S. Cai, C. and P. Albrecht. Flutter derivatives based random parametric excitation aerodynamic analysis. *Computers and Structures*, pages 463–477, 2000.

[2] S. R. Chen and C. S. Cai. Evolution of long-span bridge response to wind-numerical simulation and discussion. *Computers & Structures*, pages 2055–2066, 2003.

[3] E. Conti et al. Wind effects on the normandie cable-stayed bridge: comparison between full aeroelastic model tests and quasi-steady analytical approach. In *International Conference A.I.P.C.-F.I.P.: Cable-Stayed and Suspension Bridges*, volume 2, pages 81–91. Deauville, 1994.

[4] C. E. N. Mazzilli, J. C. André, and M. E. S. Soares. A simple numerical model for the aeroelastic analysis of cable-stayed bridges. In *Jubileum Conference On Wind Effects on Buildins and Structures. Proceeding, Roterdam, A. A. Balkema*, volume 2, pages 37–44, 1998.

[5] J. P. R. Nicoló. Seleção modal para a construção de modelos matemáticos reduzidos visando à análise do drapejamento em pontes suspensas. *Dissertação de Mestrado da Universidade de São Paulo*, 2002.

[6] I. B. Ramos. Modelos matemáticos simples para análise aeroelástica de ponte estaiadas e de pontes pênseis: desprendimento de vórtices e drapejamento. *Dissertação de Mestrado da Universidade de São Paulo*, 1999.

[7] E. Simiu and R. H. Scanlan. *Wind effects on structures: fundamentals and application design.* John Wiley & Sons, New York, 1996.

[8] M. Virlogeux et al. Design of the normandie bridge. In *International Conference A.I.P.C.-F.I.P.: Cable-Stayed and Suapension Bridges*, volume 1, pages 605–630. Deauville, 1994.